

Thermal Property of $Y_{4.67}(\text{SiO}_4)_3\text{O}$ Ceramic Sintered from Hydrothermally Synthesized Spindle-like $Y_{4.67}(\text{SiO}_4)_3\text{O}$ Apatite Crystallites

WANG Qing-Gang¹, HUANG Jian-Feng¹, ZHOU Lei^{1,2}, WU Wan-Chen¹, CAO Li-Yun¹

(1. School of Material Science and Engineering, Shaanxi University of Science and Technology, Xi'an 710021, China; 2. State Key Laboratory of Solidification Processing, Northwestern Polytechnical University, Xi'an 710072, China)

Abstract: Spindle-like $Y_{4.67}(\text{SiO}_4)_3\text{O}$ apatite crystallites composed of numerous nanoparticles with a mean diameter of about 50 nm were synthesized *via* a facile hydrothermal method at 503 K for 12 h. To the best of our knowledge, the thermal properties of the spindle-like $Y_{4.67}(\text{SiO}_4)_3\text{O}$ apatite crystallites was firstly reported. Their phase composition, microstructure, formation mechanism were investigated. Results show that hydrothermal temperature greatly influences the crystal phase composition and the crystal morphology. In addition, the obtained $Y_{4.67}(\text{SiO}_4)_3\text{O}$ ceramics possess low thermal conductivity and a relatively high thermal expansion coefficient, which make them a promising candidate material for environmental/thermal barrier coatings.

Key words: ceramics; $Y_{4.67}(\text{SiO}_4)_3\text{O}$ apatite crystallites; thermal properties

Silicon-based ceramics are prime candidates to use in the next generation gas turbine engines owing to their superior high-temperature strength and creep resistance^[1-2]. However, the poor environmental durability in combustion environments limits the applications of these materials^[3]. Applying environmental barrier coatings (EBC) or thermal barrier coatings (TBC) has been proved as an effective method for addressing this issue^[4-7].

Recently, yttrium silicates have been proven as promising candidates for EBC due to their low thermal conductivity, good thermal and chemical stability, and similar thermal expansion coefficient with silicon-based ceramics^[8-10]. There are three ternary crystal phases, namely $Y_2\text{SiO}_5$, $Y_2\text{Si}_2\text{O}_7$ and $Y_{4.67}(\text{SiO}_4)_3\text{O}$ in the binary $Y_2\text{O}_3$ - SiO_2 system^[11]. In particular, γ - $Y_2\text{Si}_2\text{O}_7$ and X2- $Y_2\text{SiO}_5$ have been studied thoroughly. γ - $Y_2\text{Si}_2\text{O}_7$ and X2- $Y_2\text{SiO}_5$ have complementary linear CTEs ($(3.90 \pm 0.4) \times 10^{-6} \text{ K}^{-1}$ for γ - $Y_2\text{Si}_2\text{O}_7$ and $8.36 \times 10^{-6} \text{ K}^{-1}$ for X2- $Y_2\text{SiO}_5$) and low thermal conductivity ($<3 \text{ W}/(\text{m} \cdot \text{K})$) above 573 K for γ - $Y_2\text{Si}_2\text{O}_7$ and $\sim 1.6 \text{ W}/(\text{m} \cdot \text{K})$ for $Y_2\text{SiO}_5$ ^[12-13]. However, few works report the thermal properties of $Y_{4.67}(\text{SiO}_4)_3\text{O}$ due to the difficulty to synthesize stoichiometric and single phase of the $Y_{4.67}(\text{SiO}_4)_3\text{O}$. Thus, it is worthy to make clear the thermal properties of the $Y_{4.67}(\text{SiO}_4)_3\text{O}$.

In the present work, the spindle-like $Y_{4.67}(\text{SiO}_4)_3\text{O}$ apatite crystallites have been successfully prepared *via* a

facile hydrothermal method. The phase composition, microstructure, formation mechanism and thermal properties of the $Y_{4.67}(\text{SiO}_4)_3\text{O}$ were investigated.

1 Experimental

1.1 Synthesis of $Y_{4.67}(\text{SiO}_4)_3\text{O}$ apatite crystallites

The typical synthesis route of $Y_{4.67}(\text{SiO}_4)_3\text{O}$ is given as follows: firstly, 1.1490 g $Y(\text{NO}_3)_3 \cdot 6\text{H}_2\text{O}$ and 0.6395 g $\text{Na}_2\text{SiO}_3 \cdot 9\text{H}_2\text{O}$ were dissolved in 10 mL distilled water under magnetic stirring to form transparent solutions, separately. Secondly, Na_2SiO_3 solution was slowly dropped into $Y(\text{NO}_3)_3$ solution under intense stirring. Then 6 mol/L of NaOH was added dropwise with magnetic stirring to adjust the pH value of the resulting solution to 13, forming the precursor solution. Thirdly, after stirring for 3 h, the precursor solution was sealed in a 100 mL Teflon-lined stainless-steel autoclave linear with a filling ratio of 30% and was slowly heated to a proper temperature (483 K, 493 K, 503 K) and maintained for 12 h. And then, the autoclave was naturally cooled to room temperature. After the centrifugal separation, the obtained precipitants were washed repeatedly several times with the distilled water and anhydrous ethanol. Afterwards, the precipitants were dried in vacuum drying oven at 333 K for 4 h. Finally, the $Y_{4.67}(\text{SiO}_4)_3\text{O}$ apatite crystallites were obtained.

Received date: 2017-10-20; Modified date: 2017-12-19

Foundation item: National Natural Science Foundation of China (51272146); Innovation Team Assistance Foundation of Shaanxi Province (2013KCT-06); Graduate Innovation Foundation of Shaanxi University of Science and Technology

Biography: WANG Qing-Gang (1978-), male, candidate of PhD. E-mail: 17156587@qq.com

Corresponding author: HUANG Jian-Feng, professor. E-mail: huangjfsust@126.com

1.2 Ceramic preparation

The as-prepared powders were granulated with 5wt% polyvinyl alcohol (PVA) and pressed into green disks of 12.6 mm in diameter and about 1.9 mm in thickness and a cubic with a size of 15 mm×3 mm×4 mm. They were then sintered in air at 1673 K for 5 h.

1.3 Characterization

The phase compositions were characterized by X-ray diffraction (XRD, D/max2200PC, Rigaku, Japan) at a working voltage and current of 40 kV and 40 mA. The morphology of the crystallites was observed by field emission scanning electron microscopy (FE-SEM, Hitachi S-4800, 5 kV). The microstructures of the samples were observed by transmission electron microscopy (TEM, JEM-3010) and high-resolution transmission electron microscopy (HRTEM). Selected area electron diffraction (SAED) patterns were recorded by a Gatan CCD camera in a digital format. Thermogravimetry-differential scanning calorimeter (TG-DSC) measurements were conducted on the as-prepared $Y_{4.67}(\text{SiO}_4)_3\text{O}$ powders using a thermo gravimetric analyzer (STA449F3, Netzsch, Germany). The powder samples were heated in N_2 atmosphere at a rate of 10 K/min up to 1473 K.

The thermal diffusivity (α) of the sintered samples was carried out on disk-shaped specimens (ϕ 12.6 mm × 1.9 mm). Both the front and back faces of the specimen were coated with a thin layer of graphite. Values for the specific heat capacity were obtained from an investigation of powder specimens using DSC (204F1, Netzsch) in N_2 atmosphere.

The thermal conductivity k was calculated by Eq. (1) with the thermal diffusivity (α), the specific heat capacity (C_p) and density (ρ) as follows.

$$k = C_p \cdot \alpha \cdot \rho \quad (1)$$

The actual thermal conductivity of the samples k_0 was further normalized by Eq. (2)^[14]:

$$\frac{k}{k_0} = 1 - \frac{4}{3}\phi \quad (2)$$

Where ϕ is the porosity of the sintered specimen, which was measured by mercury analyzer (AutoPore IV 9500).

The thermal expansion coefficient (CTE) of the sintered specimen was recorded with a high-temperature dilatometer (DIL402PC, Netzsch).

2 Results and discussion

XRD patterns of $Y_{4.67}(\text{SiO}_4)_3\text{O}$ apatite crystallites prepared by the hydrothermal method are shown in Fig. 1. At 483 K, the powders are amorphous. With the increase

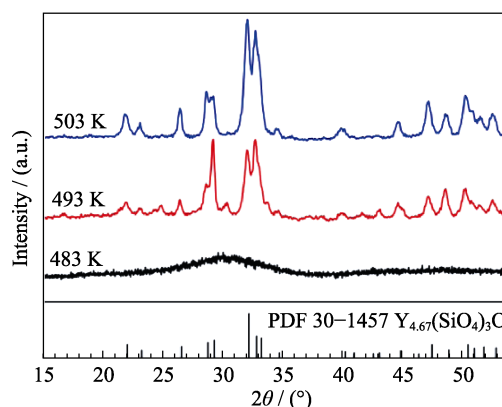


Fig. 1 XRD patterns of $Y_{4.67}(\text{SiO}_4)_3\text{O}$ at different temperatures after reaction for 12 h

of hydrothermal temperature to 493 K, the main phases of $Y_{4.67}(\text{SiO}_4)_3\text{O}$ (PDF 30-1457) can be found. Nonetheless, a few diffraction peaks of impurities are also found. Upon raising the temperature to 503 K, the monophase of $Y_{4.67}(\text{SiO}_4)_3\text{O}$ with the strong and integrate diffraction peaks was achieved, which indicates that higher hydrothermal temperature favor the pure crystalline phase of $Y_{4.67}(\text{SiO}_4)_3\text{O}$ apatite crystallites with better crystallization.

Fig. 2 shows SEM images of the samples resulted from different hydrothermal temperatures. At 483 K, it can be observed that the product was formed by irregular spherical nanoparticles (Fig. 2(a)). With the increase of temperature to 493 K, nanoparticles were found to be attached with each other to form underdeveloped spindle-like structures as shown in Fig. 2(b). When the temperature increased to 503 K, $Y_{4.67}(\text{SiO}_4)_3\text{O}$ powders displayed a regular spindle-like 3D nanostructures morphology due to the conglomeration of the nanoparticles (Fig. 2(c)). Quantification of the EDS peaks gives the atomic ratios of Y : Si : O is about 4.74 : 2.75 : 13.17 (Fig. 2(d)), which is approximately consistent with the atomic ratios of $Y_{4.67}(\text{SiO}_4)_3\text{O}$. To visually observe the spindle-like nanostructures growth process, a schematic illustration of the development of self assembled spindle-like nanostructures is shown in Fig. 2(e). The formation mechanism for the spindle-like $Y_{4.67}(\text{SiO}_4)_3\text{O}$ apatite crystallites can be simply depicted as ‘self-assembly’ and oriented attachment^[15]. At 483 K, $Y_{4.67}(\text{SiO}_4)_3\text{O}$ nuclei were produced, and then grew into nanoparticles. When the synthesis temperature was elevated (493 K), the individual nanoparticles were attached side-by-side to assemble into bundles. At a high temperature (503 K), the activity of monomers was improved, which would facilitate higher probability of collision of the monomers. As a result, 3D spindle-like structure was ultimately formed by the continuous attachment of the $Y_{4.67}(\text{SiO}_4)_3\text{O}$ nanoparticles at 503 K.

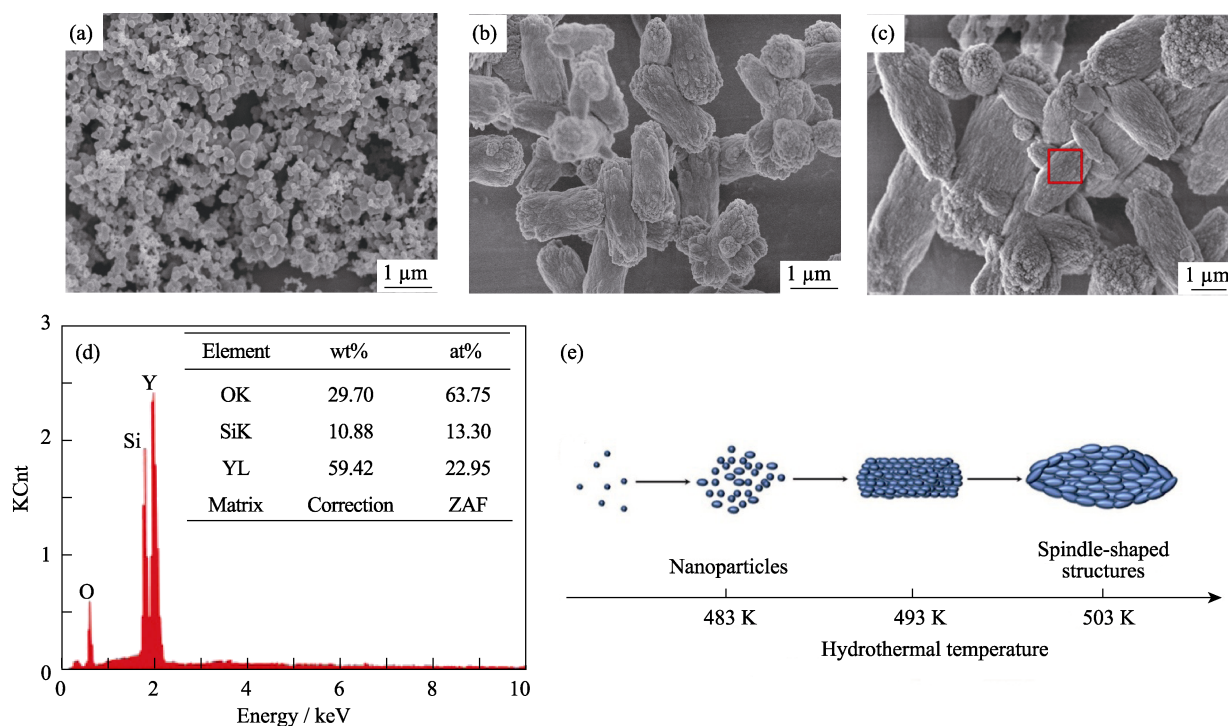


Fig. 2 SEM images of the products synthesized at different temperatures (a) 483 K; (b) 493 K; (c) 503 K; (d) EDS analysis spectrum of the $Y_{4.67}(\text{SiO}_4)_3\text{O}$; (e) Schematic diagram of the growth process of the spindle-like $Y_{4.67}(\text{SiO}_4)_3\text{O}$ apatite crystallites

Fig. 3 shows transmission electron microscopy (TEM) of the synthesized $Y_{4.67}(\text{SiO}_4)_3\text{O}$. The overview image of $Y_{4.67}(\text{SiO}_4)_3\text{O}$, shown in Fig. 3(a), illustrating that the as-obtained product possesses the spindle-like structures, which actually being composed of numerous nanoparticles with a mean diameter of about 50 nm (Fig. 3(b)). Fig. 3(c) presents the HRTEM image of the $Y_{4.67}(\text{SiO}_4)_3\text{O}$. The interplanar spacing of 0.340 nm and 0.278 nm are corresponding well to (002) and (211) lattice planes of the $Y_{4.67}(\text{SiO}_4)_3\text{O}$ respectively. The SAED pattern (Fig. 3(d)) demonstrates that the $Y_{4.67}(\text{SiO}_4)_3\text{O}$ has a polycrystalline feature.

The TG-DSC curves of the sample prepared at 503 K are shown in Fig. 4(a). As the measurement temperature increased, the continuous weight loss without any obvious exothermic or endothermic peaks is observed. After 1073 K, almost no weight loss can be found. The weight loss may be due to the evaporation of water and other volatile impurities. There are no decomposition and phase transformation according to the TG-DSC curves. Fig. 4(b) shows XRD patterns of $Y_{4.67}(\text{SiO}_4)_3\text{O}$ before and after sintering in air at 1673 K for 5 h respectively. No variation occurred after sintering because all of the peaks could be designated to the $Y_{4.67}(\text{SiO}_4)_3\text{O}$ crystallites though the increased peak intensity. These results demonstrate that $Y_{4.67}(\text{SiO}_4)_3\text{O}$ powders possess both thermal and structural stability under such conditions.

The microstructure of the surface of $Y_{4.67}(\text{SiO}_4)_3\text{O}$ ceramic after sintering in air at 1673 K for 5 h is shown in Fig. 4(c). The microstructure of the sintered specimen is relatively dense and only a few residual small pores can be detected at the grain boundaries. The influence of porosity can be eliminated according to Eq. (2).

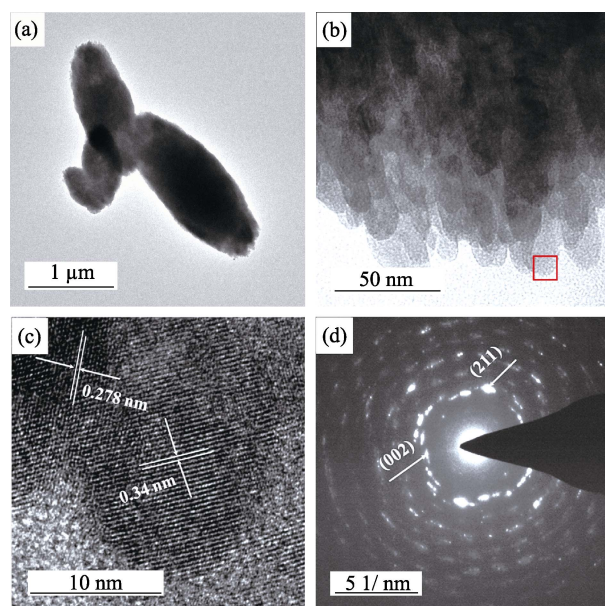


Fig. 3 TEM images of $Y_{4.67}(\text{SiO}_4)_3\text{O}$. (a) Typical TEM image; (b) Magnified image of (a); (c) High-resolution TEM image of a part of the sample; (d) Selected area electronic diffraction (SAED) pattern of (c)

The thermal conductivity and thermal expansion coefficient of $Y_{4.67}(\text{SiO}_4)_3\text{O}$ as a function of temperature are plotted in Fig. 4(d) and (e) respectively. As shown in Fig. 4(d), its thermal conductivity was about $1.2 \text{ W}/(\text{m}\cdot\text{K})$ over an elevated temperature range, which is close to that of $\text{RE}_{9.33}(\text{SiO}_4)_6\text{O}_2$ silicate oxyapatite^[16]. The low thermal conductivity of $Y_{4.67}(\text{SiO}_4)_3\text{O}$ makes it interesting for applications in EBC/TBC coatings. Fig. 4(e) illustrates the thermal expansion coefficient of $Y_{4.67}(\text{SiO}_4)_3\text{O}$ ceramic measured in the temperature range of 293 K-1373 K. In the temperature range of 473 K-1373 K, the average thermal expansion coefficient is $8.02 \times 10^{-6} \text{ K}^{-1}$, which is higher than that of single-phase $\gamma\text{-Y}_2\text{Si}_2\text{O}_7$ ($(3.90 \pm 0.4) \times$

10^{-6} K^{-1})^[12] and close to single-phase polycrystalline $\text{X}_2\text{-Y}_2\text{SiO}_5$ ($8.36 \times 10^{-6} \text{ K}^{-1}$)^[13]. In addition, it agrees well with the experimental result of Thomas S. Key's report^[17].

3 Conclusion

A spindle-like $Y_{4.67}(\text{SiO}_4)_3\text{O}$ apatite crystallites have been successfully prepared *via* a facile hydrothermal method. The spindle-like $Y_{4.67}(\text{SiO}_4)_3\text{O}$ apatite crystallites were formed by numerous nanoparticles with a mean diameter of about 50 nm. There were no phase transition from room temperature to 1673 K, which indicates that

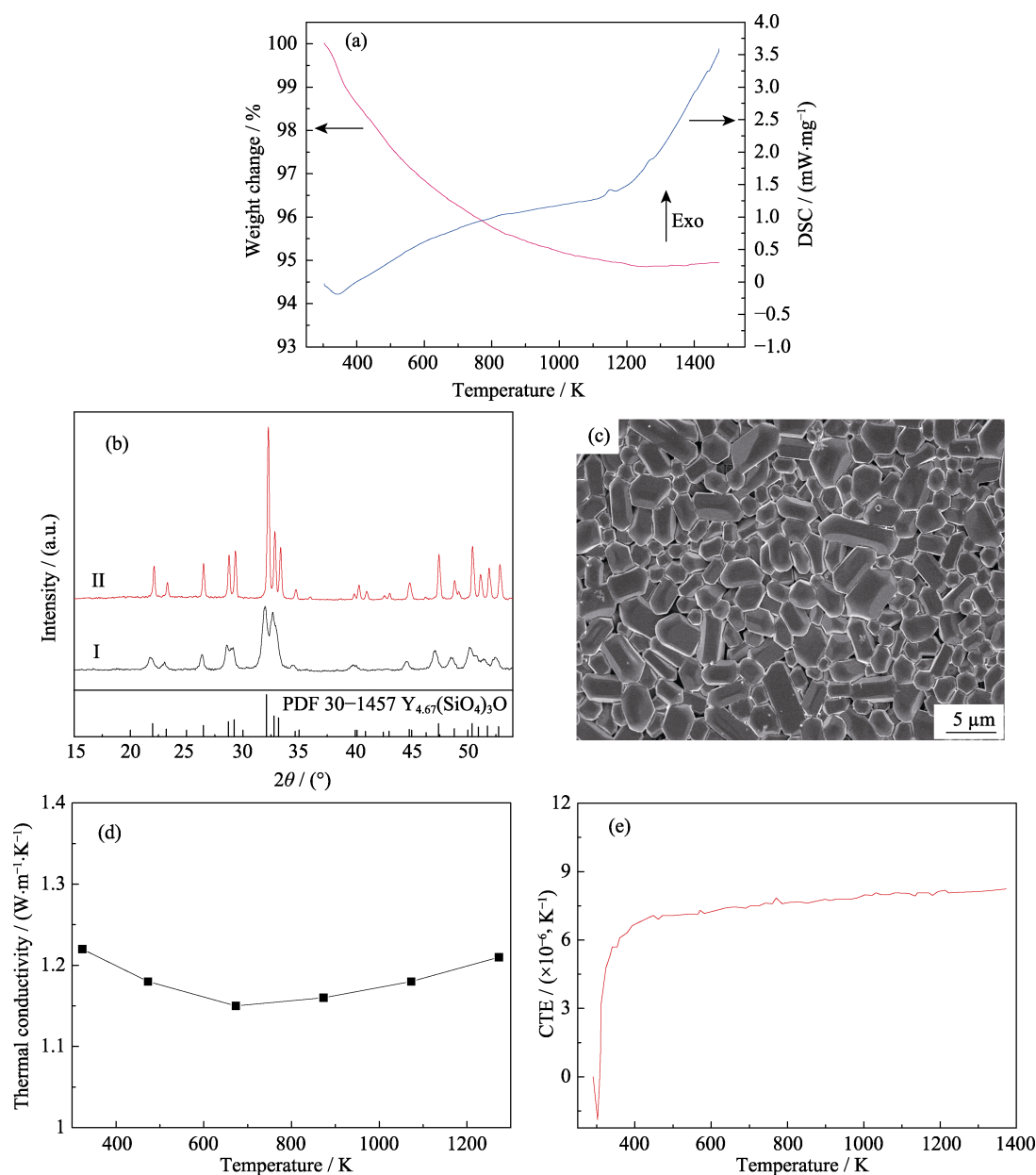


Fig. 4 Thermal properties of the sample. (a) TG-DSC curves of the $Y_{4.67}(\text{SiO}_4)_3\text{O}$ powders prepared at 503 K for 12 h; (b) XRD patterns of the sample (I) before and (II) after sintering in air for 5 h at 1673 K; (c) Microstructure of the surface of $Y_{4.67}(\text{SiO}_4)_3\text{O}$ after sintering in air for 5 h at 1673 K; (d) Thermal conductivity of $Y_{4.67}(\text{SiO}_4)_3\text{O}$ ceramics; (e) Thermal expansion coefficients of $Y_{4.67}(\text{SiO}_4)_3\text{O}$ ceramics

$Y_{4.67}(SiO_4)_3O$ powders possess both thermal and structural stability. $Y_{4.67}(SiO_4)_3O$ ceramic has a lower thermal conductivity ($1.2 \text{ W/(m}\cdot\text{K)}$) over an elevated temperature range. Moreover, $Y_{4.67}(SiO_4)_3O$ has relatively high thermal expansion coefficient ($8.02 \times 10^{-6} \text{ K}^{-1}$) in the temperature range of 473 K–1373 K. These good thermal properties make them a potential candidate for environmental/ thermal barrier coating materials.

References:

- [1] KLEMM HAGEN, TAUT CHRISTINE, WOTTING GERHARD. Long-term stability of nonoxide ceramics in an oxidative environment at 1500°C . *Journal of the European Ceramic Society*, 2003, **23**(4): 619–627.
- [2] XU YUE, HU XUN-XUN, XU FANG-FANG, *et al.* Rare earth silicate environmental barrier coatings: present status and prospective. *Ceramics International*, 2017, **43**(8): 5847–5855.
- [3] MORE KARREN L, TORTORELLI PETER F, WALKER LARRY R, *et al.* High temperature stability of SiC-based composites in high-water-vapor-pressure environments. *Journal of the American Ceramic Society*, 2003, **86**(8): 1272–1281.
- [4] STOLZENBURG F, KENESEI P, ALMER J, *et al.* The influence of calcium-magnesium-aluminosilicate deposits on internal stresses in $Yb_2Si_2O_7$ multilayer environmental barrier coatings. *Acta Materialia*, 2016, **105**: 189–198.
- [5] WANG CHAO, CHEN MENG, WANG HONG-JIE, *et al.* Fabrication and thermal shock resistance of multilayer γ - $Y_2Si_2O_7$ environmental barrier coating on porous Si_3N_4 ceramic. *Journal of the European Ceramic Society*, 2016, **36**(3): 689–695.
- [6] AL NASIRI N, PATRA N, JAYASEELAN D D, *et al.* Water vapour corrosion of rare earth monosilicates for environmental barrier coating application. *Ceramics International*, 2017, **43**(10): 7393–7400.
- [7] WANG YI-GUANG, WU YA-HUI, CHENG LAI-FEI, *et al.* Hot corrosion behavior of barium aluminosilicate-coated C/SiC composites at 900°C . *Journal of the American Ceramic Society*, 2009, **93**(1): 204–208.
- [8] SEIFERT HANS J, WAGNER SIGRID, FABRICHNAYA OLGA, *et al.* Yttrium silicate coatings on chemical vapor deposition-SiC-precoated C/C-SiC: thermodynamic assessment and high-temperature investigation. *Journal of the American Ceramic Society*, 2005, **88**(2): 424–430.
- [9] LEE KANG N, FOX DENNIS S, BANSAL NAROTTAM P. Rare earth silicate environmental barrier coatings for SiC/SiC composites and Si_3N_4 ceramics. *Journal of the European Ceramic Society*, 2005, **25**(10): 1081–1088.
- [10] MA QING-SONG, CAI LI-HUI. Fabrication of $Y_2Si_2O_7$ coating and its oxidation protection for C/SiC composites. *Transactions of Nonferrous Metals Society of China*, 2017, **27**(2): 390–396.
- [11] SUN ZI-QI, LI MEI-SHUANG, ZHOU YAN-CHUN. Recent progress on synthesis, multi-scale structure, and properties of Y-Si-O oxides. *International Materials Reviews*, 2014, **59**(7): 357–383.
- [12] SUN ZI-QI, ZHOU YAN-CHUN, WANG JING-YANG, *et al.* Thermal properties and thermal shock resistance of γ - $Y_2Si_2O_7$. *Journal of the American Ceramic Society*, 2008, **91**(8): 2623–2629.
- [13] SUN ZI-QI, LI MEI-SHUANG, ZHOU YAN-CHUN. Thermal properties of single-phase Y_2SiO_5 . *Journal of the European Ceramic Society*, 2009, **29**(4): 551–557.
- [14] XU ZHEN-HUA, HE LI-MIN, MU REN-DE, *et al.* $(Y_{0.05}La_{0.95})_2(Zr_{0.7}Ce_{0.3})_2O_7$ ceramics as a thermal barrier coating material for high-temperature applications. *Materials Letters*, 2014, **116**(2): 182–184.
- [15] MAO CHANG-JIE, PAN HONG-CHENG, WU XING-CAI, *et al.* Sonochemical route for self-assembled V_2O_5 bundles with spindle-like morphology and their novel application in serum albumin sensing. *Journal of Physical Chemistry B*, 2006, **110**(30): 14709–14713.
- [16] WU RUI-FEN, PAN WEI, REN XIAO-RUI, *et al.* An extremely low thermal conduction ceramic: $Re_{9.33}(SiO_4)_6O_2$ silicate oxyapatite. *Acta Materialia*, 2012, **60**: 5536–5544.
- [17] KEY THOMAS S, PRESLEY KAYLA F, HAY RANDALL S, *et al.* Total thermal expansion coefficients of the yttrium silicate apatite phase $Y_{4.69}(SiO_4)_3O$. *Journal of the American Ceramic Society*, 2014, **97**(1): 28–31.

水热法制备纺锤型磷灰石相 $Y_{4.67}(SiO_4)_3O$ 微晶及其陶瓷的热学性能研究

汪庆刚¹, 黄剑锋¹, 周磊^{1,2}, 仵婉晨¹, 曹丽云¹

(1. 陕西科技大学 材料科学与工程学院, 西安 710021; 2. 西北工业大学 凝固技术国家重点实验室, 西安 710072)

摘要: 采用水热法在温度为 503 K, 反应时间为 12 h 的条件下制备了纺锤型磷灰石相 $Y_{4.67}(SiO_4)_3O$ 微晶, 该微晶由粒径约为 50 nm 的颗粒组成。首次报道了纺锤型磷灰石相 $Y_{4.67}(SiO_4)_3O$ 微晶的热性能, 同时研究了其相组成, 微观结构及合成机理。结果表明, 水热温度对所制备粉体的相组成及形貌有较大影响。此外, 对应的陶瓷具有较低的热导率和较高的热膨胀系数, 有望用作热障/环障涂层材料。

关键词: 陶瓷; 磷灰石相 $Y_{4.67}(SiO_4)_3O$ 微晶; 热学性能

中图分类号: TQ174 文献标识码: A